INTERNATIONAL JOURNAL FOR NUMERICAL METHODS IN FLUIDS
Int. J. Numer. Meth. Fluids 2011; **67**:651–670
Published online 21 July 2010 in Wiley Online Library (wileyonlinelibrary.com). DOI: 10.1002/fld.2383

An efficient method for discretizing 3D fractured media for subsurface flow and transport simulations

Hussein Mustapha[1,*,†], Roussos Dimitrakopoulos[1], Thomas Graf[2] and Abbas Firoozabadi[3,4]

[1]*Department of Mining and Materials Engineering, McGill University, Montreal, Canada H3A 2A7*
[2]*Institute of Fluid Mechanics in Civil Engineering, Leibniz Universität Hannover, Hannover, Germany*
[3]*Reservoir Engineering Research Institute, Palo Alto, CA, U.S.A.*
[4]*Yale University, New Haven, CT, U.S.A.*

SUMMARY

We introduce a new method to discretize inclined non-planar two-dimensional (2D) fractures in three-dimensional (3D) fractured media for subsurface flow and transport simulations. The 2D fractures are represented by ellipsoids. We first discretize the fractures and generate a 2D finite element mesh for each fracture. Then, the mesh of fractures is analyzed by searching and treating critical geometric configurations. Based on that search, the method generates a quality mesh and allows for including finer grids. A solute transport problem in fractured porous media is solved to test the method. The results show that the method (i) adequately represents the fractured domain by maintaining the geometric integrity of input surfaces and geologic data, (ii) provides accurate results for both simple and complex fractured domains, (iii) is insensitive to spatial discretization, and (iv) is computationally very efficient. For inclined and vertical fractures, analytical and numerical solutions are shown to be in good agreement. The method is therefore suitable to discretize fracture networks for flow and transport simulations in fractured porous media.

Received 29 January 2010; Revised 27 May 2010; Accepted 28 May 2010

KEY WORDS: 3D discrete-fractured model; mesh generation; adaptive mesh; flow and transport

1. INTRODUCTION

Fractured media are multi-scale heterogeneous and contain highly complex geologic configurations [1–6]. The complexities are mainly because of a large number of fractures and strong variations in physical and geometric properties, such as permeability, aperture, length, orientation, position and shape. Fractures in rock formations may have a significant effect on multiphase flow and solute transport [7–9]. For example, fractures represent preferential pathways where solutes migrate at velocities that are several orders of magnitude larger than within the rock matrix itself [1–9]. An efficient and accurate discretization of these fractures within the matrix is required to account for the natural complexity of fractured media and the physics of matrix–fracture interaction. Mesh generation or fracture disctretization refers to generating solid finite element meshes representing the heterogeneous media, which are used to solve various engineering problems based on finite element methods. Generating a quality mesh is equally important for multiphase flow problem simulations [10–12].

*Correspondence to: Hussein Mustapha, Department of Mining and Materials Engineering, McGill University, 3450 University Street, Montreal, Canada H3A 2A7.
†E-mail: hussein.mustapha@mcgill.ca

Fractured media with regularly distributed fractures and limited number of fractures are studied by several authors [13–16]. However, fractured media simulations often require representation of complex, irregular domains and complicated fracture networks. Different approaches to represent complex geometry of fractured media have been used in past flow studies in discretely fractured media. A thorough discussion of discretization approaches is provided by Graf and Therrien [17], which is briefly reiterated. The matrix is assumed to be impermeable in some studies [18–21] where flow only takes place along one-dimensional (1D) intersections of two-dimensional (2D) fractures. An impermeable matrix simplifies fracture discretization because only the 2D fractures require discretization. However, the low-permeability porous matrix cannot be neglected for solute transport and/or for CO_2 sequestration studies because of potentially high diffusive fluxes within the rock matrix [17]. A '2.75D' mesh generation of discretely fractured media has been proposed in [22]. The method discretizes fractures by 2D elements and subdivides the low-permeability porous matrix into two regions: a region near fractures and a region far from fractures. Steady-state conditions are assumed in the second region, making its representation in the grid unnecessary. Transient conditions are assumed in the first region and the porous matrix near the fractures is discretized either by three-dimensional (3D) prisms or 3D hexahedra. A network of 3D matrix elements covering 2D fractures is obtained using the '2.75D' proposed mesh. The method is useful to simulate flow and transport in fractures and parts of the matrix. However, simulations of different stochastic realizations of fractured media cannot be achieved using a reasonable time frame because each simulation requires time-consuming remeshing of the '2.75D' domain. Various authors have used orthogonal grids allowing only for representation of orthogonal discrete fractures [23–25]. Inclined fractures have been discretized on orthogonal grids by combining horizontal and vertical 1D fracture elements that connect element-centered nodes of adjoining 2D porous matrix elements [26, 27]. A different technique has been used to discretize arbitrarily inclined non-planar triangulated fractures in 3D orthogonal grids by combining horizontal and vertical rectangular fracture elements [28]. In the alternative technique, the fracture surface area is increased which can influence simulation result because flow paths are different. Recently, a new method to discretize non-planar inclined discrete fracture is introduced in [17]. That technique discretizes the porous media into tetrahedrons, and then approximates the embedded fractures by the faces of these tetrahedrons. Reference [17] and most of the methods cited above are designed to discretize complex fractured media; however, they have been used for simple fractured configurations where a simplification procedure is mostly not needed. Moreover, these methods are mainly based on a non-optimal and global transformation of the fractures which is used to reduce complex configurations; furthermore, they cannot generate fine grids. Blessent *et al.* [29] have developed a new method to discretize non-planar fractures. They have generated fine triangles close to fractures and coarse elements away from fractures. Their approach generates fine tetrahedrons close to fractures and identifies certain tetrahedron faces as fracture faces. That method efficiently approximates single-fracture configuration. However, the method becomes computationally costly and difficult to implement for complex fractured media.

Stochastically generated fractures lead to complex geometric configurations in 2D and in 3D spaces as shown in Figure 1. The mesh generation of these configurations is constrained by several

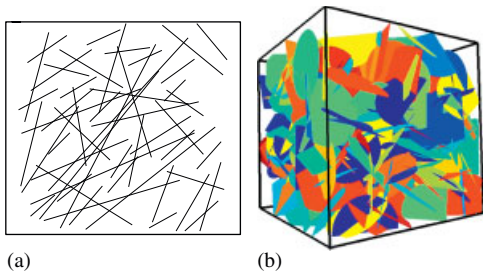

Figure 1. Discrete-fractured media generated stochastically (a) in 2D [30] and (b) in 3D [21]. In 2D, the fractures are represented by segments; they are modelled by ellipsoids in 3D.

DOI: 10.1002/fld

randomly located fractures. In addition, large statistical sets of generated fractures have to be discretized. This requires a robust and fully automated meshing algorithm.

In this work, we extend the 2D approach developed in [30] to 3D. The basic idea is to locally transform the complex and critical geometric configurations of fractured media. Based on given criteria, the critical (i.e. geometrically complex) configurations are first searched. Then, these configurations are locally analyzed with a minimal number of modifications. Consequently, the structure of globally connected fractures is mostly unchanged. The removal of complex configurations helps to generate a mesh quality with a small error in the numerical solution.

2. MESH GENERATION IN 3D FRACTURED MEDIA

2.1. Mesh generation methods

Structured mesh generation is mostly devoted for orthogonal and regularly distributed fractures. However, complex fractured media contain irregular fractures, and triangle and tetrahedral meshing are the most common forms of unstructured mesh generation. Most meshing techniques that use triangles and tetrahedrons are based on the Delaunay [31] criterion. The Delaunay criterion is not an algorithm to generate a mesh, but it provides the criteria to connect a set of existing points in space. It is therefore necessary to provide a method to generate node locations in space. A typical approach is to first mesh the boundary of the geometry to provide an initial set of nodes. The boundary nodes are then triangulated according to the Delaunay criterion. Nodes are then inserted incrementally into the existing mesh, locally redefining the triangles or tetrahedrons as each new node is inserted to satisfy the Delaunay criterion. This is the method that is chosen for defining where to locate the interior nodes that distinguish one Delaunay algorithm from another.

There are many different Delaunay triangulation methods based on divide-and-conquer and gift-wrapping methods [32, 33]. However, incremental methods are the most popular Delaunay meshing techniques. Incremental methods start with an initial mesh (usually a boundary conforming mesh), which is refined incrementally by inserting new points (one at a time) using a spatial distribution technique. Each new point is re-connected with the existing points of the mesh in order to form a new triangulation or a new mesh. The differences between the various Delaunay incremental algorithms in the literature are: (1) different spatial point distribution methods for creating the points and (2) different local reconnection techniques for creating triangles or tetrahedrons. For more details, the reader is referred to [10]. Many finite element applications require that an existing surface triangulation be maintained, i.e. the triangulation of the fractures in Figure 1(b). Then, the triangulation may no longer be strictly 'Delaunay', and is called in this case 'Boundary Constrained Delaunay Triangulation' [10].

2.2. Discussion on mesh quality

The computational analysis of the solution quality and the time needed to obtain that solution depend on the mesh quality. Examples are poorly conditioned problems, and non-linear and/or transient analyses. Different techniques can be used to evaluate the mesh quality [10, 30] to provide some indication about the suitability of the discretization type under consideration. In this work, an elementary criterion has been adopted, which consists of an evaluation of the element quality with respect to the equilateral simplex. For a triangular element, the quality is expressed as [30]

$$q = \alpha \frac{A}{a^2 + b^2 + c^2}, \tag{1}$$

where A is the area of the triangle, a, b and c are the lengths of the sides and $\alpha = 4\sqrt{3}$ is a normalizing coefficient that gives the quality of an equilateral triangle as 1. The quality of particular triangles is shown in Figure 2.

DOI: 10.1002/fld

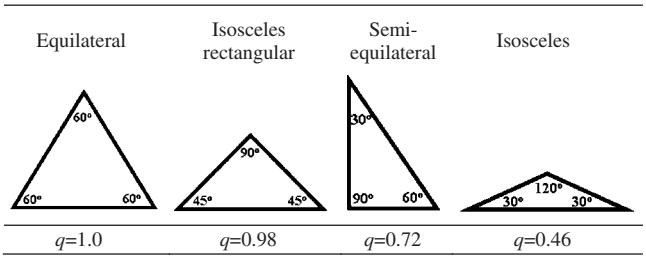

Figure 2. Triangles and their quality (q) using Equation (1) [30].

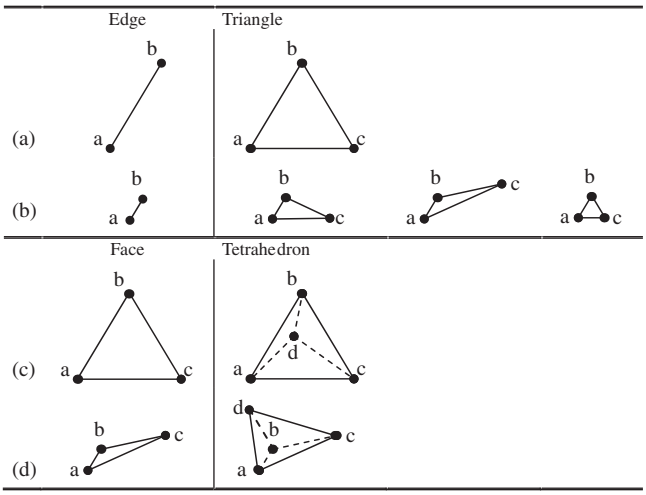

Figure 3. Effect of edges and faces' size on the quality of triangles and tetrahedrons.

A similar formula is also used to evaluate the quality of a tetrahedral element

$$q = \alpha \frac{V^2}{(a+b+c+d)^3}, \tag{2}$$

where V denotes the volume of the tetrahedron, a, b, c and d are the areas of the faces and $\alpha = 216\sqrt{3}$ is a normalizing coefficient ensuring that the quality of an equilateral tetrahedron is 1.

The above formula clearly shows that the length of an edge in a triangle and the area of a face in a tetrahedron have a considerable influence on the quality of the triangle and the tetrahedron, respectively. For example, if the length of an edge is small, a good triangle quality is obtained if the triangle area is small as shown by the last case of Figure 3(b). The triangle could be large, but its quality decreases as shown by the first two cases in Figure 3(b). A similar argument holds for the quality of the tetrahedron. However, in that case, both the edges and the faces influence tetrahedron quality. For example, Figure 3(d) shows that a low-quality face provides a low tetrahedron quality.

2.3. Simplification procedure (SP) to generate 3D complex configurations

This section presents an optimal method to discretize 3D fractured media using finite element tetrahedrons. The *optimality* of the method arises from the mesh quality obtained using fine and coarse grid levels. Mustapha and Dimitrakopoulos [30] have simplified 2D complex fracture configurations to facilitate the generation of a mesh quality without a refinement procedure to improve the mesh quality of complex fractured configurations. In that work, the 2D geometry of the fracture network is adapted instead of the 2D mesh. This work focuses on the algorithm to

DOI: 10.1002/fld

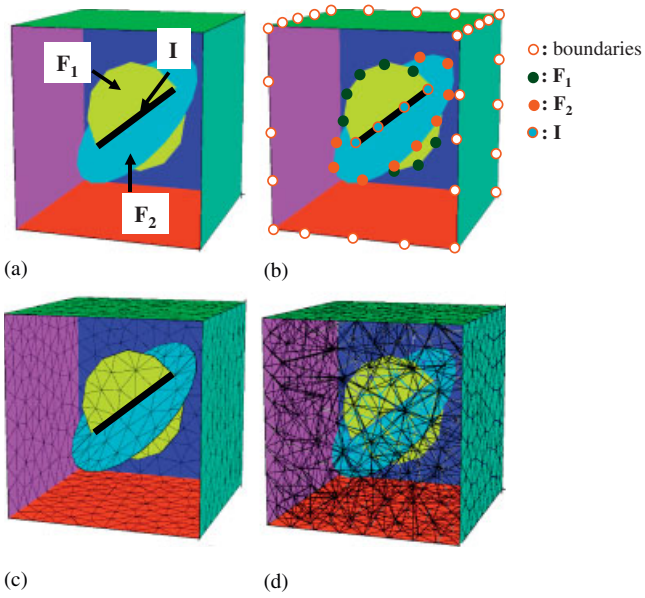

Figure 4. Discretization procedure of a two-fracture configuration (a). (b) The discretization points of the fracture borders; (c) the 2D mesh of the fractures and the boundaries of the domain; and (d) the final 3D mesh of (a).

simplify the complex fracture network configurations in 3D. A mesh quality will be generated for the simplified geometry without requiring a mesh refinement procedure. The simplification procedure (SP) will deliver an optimal solution in terms of solution precision, mesh quality and computational cost.

Consider the two-fracture configuration shown in Figure 4(a). The method developed will be described for meshing the two-fracture configuration. However, the same procedure can be used to mesh more complex geological media with any number of fractures. Denote by F_1 and F_2 the 2D fractures shown in Figure 4(a) and by $I = F_1 \cap F_2$ their intersection. Note that I is a 1D entity.

The SP method consists of four main steps that are described below:

Step 1: The boundaries of the domain and the fractures are discretized by a set of discrete points as shown in Figure 4(b). The discretization of F_1, F_2, I and the boundaries of the domain provides the set of points shown in Figure 4(b).

Step 2: The discrete points obtained in Step 1 are used to generate a 2D finite element mesh for F_1, F_2 and the boundaries of the domain as shown in Figure 4(c); the algorithm used in this step is presented in [30].

Step 3: This is the simplification procedure of SP method where all critical configurations generated by Step 2 are analyzed; it treats critical cases presented by abnormal (i.e. degenerated) triangles such as the triangle shown in Figure 3(d). In [30], the small edges are analyzed by scanning the fractured media and locally transforming the geometry. A similar technique is used here to treat critical configurations arising from small edge lengths and/or triangle areas. Close discrete points are local properties that make the gridding procedure complex. The idea is to locally reduce these complexities by keeping, as much as possible, the remaining part of the fracture network unchanged. The procedure developed consists of scanning the results from Step 2 by a small cube of size $(h' \times h' \times h')$ defined by the user. Normally $h' \leqslant h$ where h is the mesh step used in Step 1. The cube is first located at the lower-left corner of the fractured domain as shown in Figure 5(a). Then, the cube is moved along x-, y- and z-directions, respectively, as shown in Figure 5(b). The solid cube in this figure represents the current cube to be used to check for critical configurations as explained below. However, the dotted cubes were used before in the checking procedure. For a better explanation, we consider in Figure 6 the case of one cube with all possible configurations

DOI: 10.1002/fld

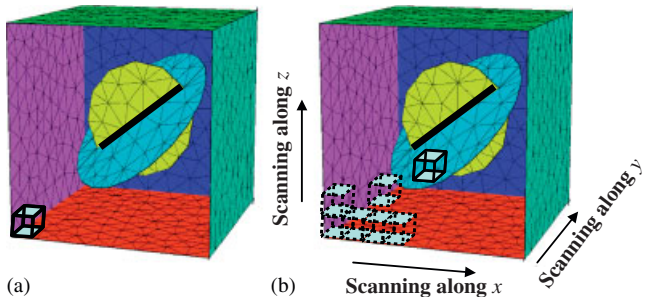

Figure 5. Scanning procedure used. (a) A small cube (size defined by the user) is located at the lower left corner of the fractured domain. The fractured domain is scanned by the small cube first along x-, then y-, and then z-directions. The dotted cubes in (b) represent some of the previously tested cubes.

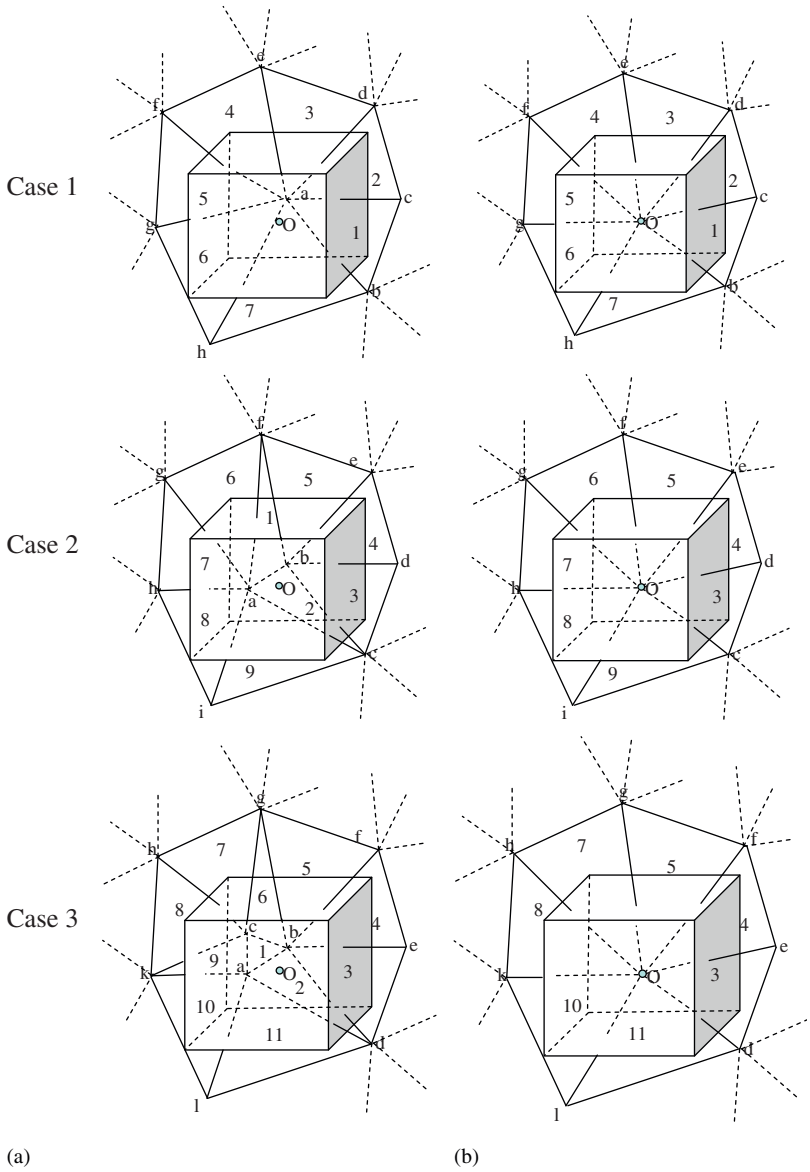

Figure 6. Local mesh transformation in (a) to obtain (b) using the SP method. Three different cases are distinguished when only one node, one edge or one triangle is inside the cube.

DOI: 10.1002/fld

that can be encountered in a 2D mesh. Different cases can be distinguished if the current cube

1. does not contain any node from the triangles generated in Step 2. Here, we move to the next cube that is known to be inactive since the beginning. Thus, the algorithm developed is optimal with respect to the number of cubes to be checked.
2. contains only one node, which is common to a set of triangles as shown in Figure 6(a), case 1. In that case, we only translate the node to coincide with the cube center as shown in Figure 6(b), case 1.
3. contains only one edge as shown in Figure 6(a), case 2. In that case, the edge (a,b) is removed and replaced by the cube center. Then, all the triangles (i.e. (1) and (2)) containing that edge are removed as shown in Figure 6(b), case 2.
4. contains a small triangle as shown by the triangle (1) in Figure 6(a), case 3. This triangle shares one edge with each of the triangles (2), (6) and (9). In that case, triangles (1), (2), (6) and (9) are removed and only replaced by the cube center. Then, the other triangles i.e. (3), (4), (5), (7), (8), (10) and (11) are joined at the cube center as shown in Figure 11(b), case 3.

Step 4: The faces (i.e. triangles) provided from Step 3 represent the base to generate tetrahedrons to fill the 3D domain in Figure 4(a). In this step, we have implemented a classic Delaunay algorithm to generate the tetrahedrons in the fractured media as shown in Figure 4(d). Note that the triangles generated within the fractures and the faces of the tetrahedrons next to the fractures coincide.

Note that any situation other than those presented in Figure 6 has to combine the three cases presented earlier, and then the procedure described above will solve the problem. Only one scan is sufficient to search the critical configurations over the entire domain. A second scan would not detect any new critical configuration, because the minimal distance between any two points within the new set of points (Figure 6(b)) is larger than $h'/2$, which is the distance between the center of a cube ($h' \times h' \times h'$) and its neighbors.

An example of meshing single-fracture configuration using the SP method is shown in Figure 7(1). Figure 7(2) compares meshes before and after simplification using a close-up in Figure 7(1) and clearly shows how the mesh is transformed locally. Note that the SP method mainly has to be applied to analyze critical configurations generated from intersections between fractures (Figure 13), and not to change internal triangle geometry far from these intersections.

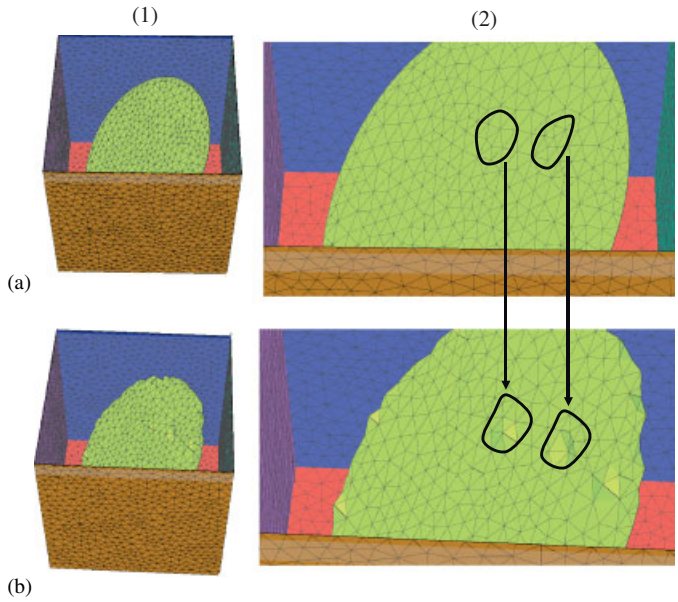

Figure 7. Single-fracture configuration meshed using the SP method. The final mesh obtained is shown in (b.1). The right side represents a close-up of both triangulations to compare the mesh after the modifications.

DOI: 10.1002/fld

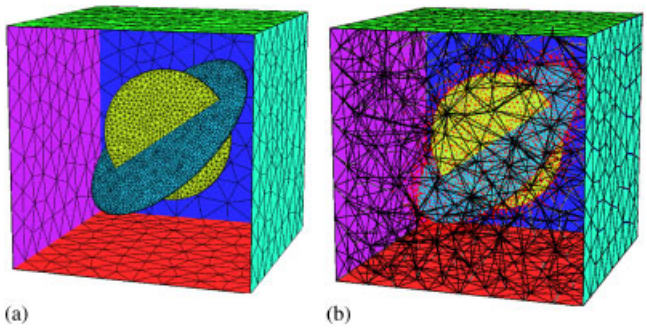

Figure 8. Different triangle areas are generated. (a) Fine triangulations of the fractures and coarse triangulations away from fractures and (b) the corresponding 3D mesh. Note that a large portion of the nodes are generated within and/or close to fractures as shown in (b).

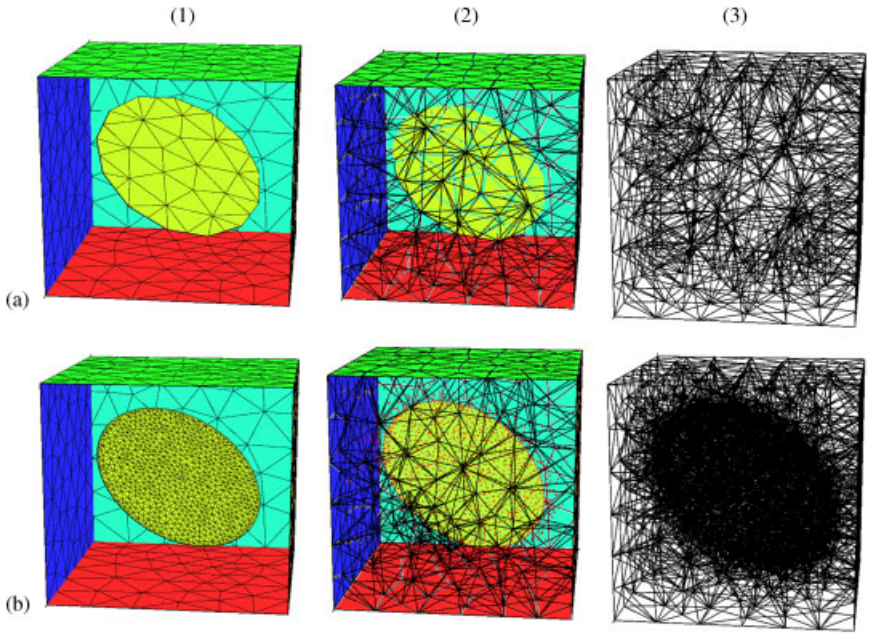

Figure 9. Mesh of single-fracture configuration. (a) Steps 2 and 4 using uniform (i.e. same discretization inside and outside fractures) discretization and (b) different discretizations inside and outside the fractures by including a refinement procedure. The third column is similar to the second column but without plotting the boundaries of the domain and the fracture.

However, it will also be useful to analyze internal critical triangles to the fractures in order to control and improve the mesh quality.

The method can generate fine triangles within the fractures and coarse triangles away from the fractures by increasing the number of points of the fracture borders in Step 1; consequently, Step 2 will generate fine triangulations of the fractures as shown in Figure 8(a). After that, the Delaunay procedure is called to generate in Step 4 the tetrahedrons as shown in Figure 8(b).

The SP method is tested in various fractured configurations, including a refinement procedure. Consider for example the simple case of a single-fracture domain shown in Figure 9. Using the algorithm presented above, Steps 2 and 4 generate a uniform triangulation in Figure 9(a.1); also, they can provide a non-uniform triangulation as shown in Figure 9(b.1) by including a refinement procedure where the discretization inside the fractures is different from elsewhere. Figure 9(3) presents the 3D mesh presented in Figure 9(2) without plotting the boundaries of the domain and the fracture. This figure clearly shows that the density of the tetrahedrons close to the fracture is

DOI: 10.1002/fld

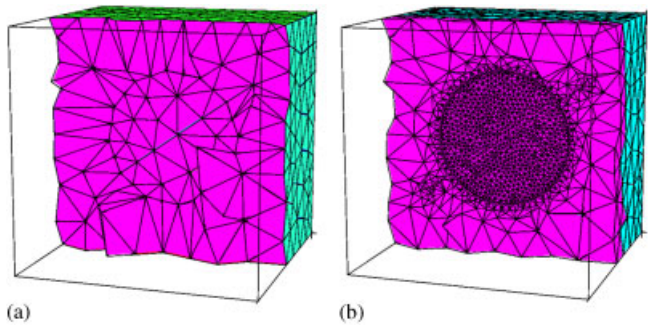

Figure 10. Cross-sections along the y-direction of Figures 4(d) and 5(b) are in (a) and (b), respectively. The clear circle in both figures refers to the vertical fracture in Figure 4(a).

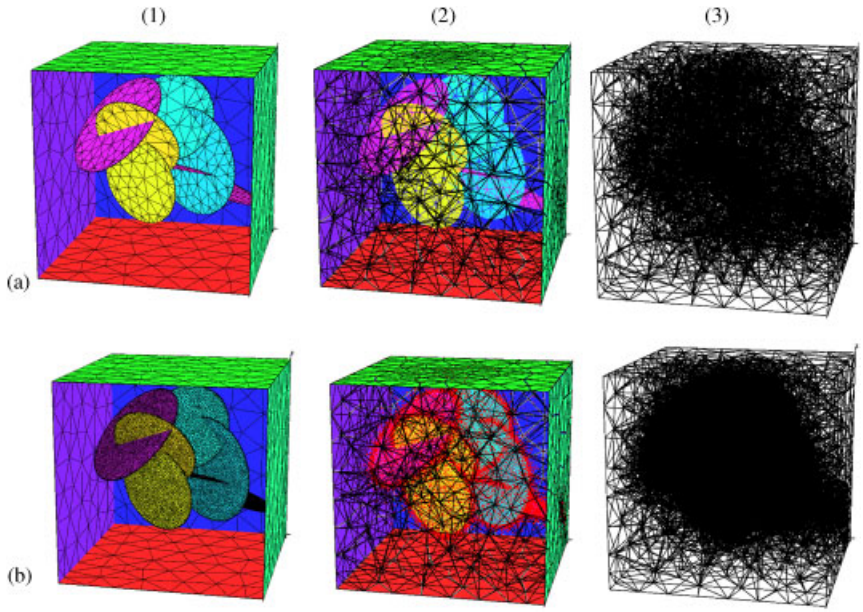

Figure 11. Mesh of a domain with six connected fractures generated stochastically. (a) Steps 2 and 4 of the method using uniform (i.e. same discretization inside and outside fractures) discretization and (b) different discretizations inside and outside the fractures by including a refinement procedure. The third column is similar to the second column but without plotting the boundaries of the domain and the fractures.

higher in Figure 9(b.3) than in Figure 9(a.3). This feature (i.e. different densities) can be clearly seen by looking at the mesh distribution in cross-sections along the y-axis of Figures 4(d) and 5(b) as presented in Figures 10(a) and 7(b), respectively. The circle shown in Figure 10 refers to the vertical fracture (approximately oriented vertically) in Figure 4(a). The cross-sections are different and show a dense region of tetrahedrons in Figure 10(a) after including a refinement procedure.

Figure 11(a.1) shows another fractured media with six connected fractures that have been generated stochastically. Different meshes are generated using the method developed as shown in Figures 11(a) and (b). The cross-sections of Figures 11(a.2) and (b.2) are presented in Figures 12(a) and (b), respectively. The figures show the ability of the method to generate fine elements inside and/or close to fractures and coarse elements away from fractures.

The 2D fractured medium generated in Figure 1 contains complex configurations mainly represented by the small angles between stochastically generated fractures. Figure 13 illustrates the case of three intersecting fractures (F_1, F_2 and F_3) where the angle between fracture intersections I_{12} (intersection between F_1 and F_2) and I_{13} (intersection between F_1 and F_3) is small (Figure 13(b)). The small angle is the main reason to generate inadequate triangles as shown in Figure 3(b),

DOI: 10.1002/fld

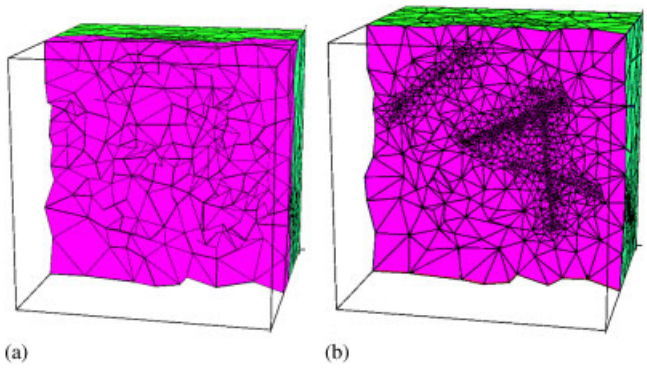

Figure 12. Cross-sections along the y-direction of Figures 8(a.2) and (b.2) in (a) and (b), respectively. The fine elements in (b) are only around the intersections between the fractures.

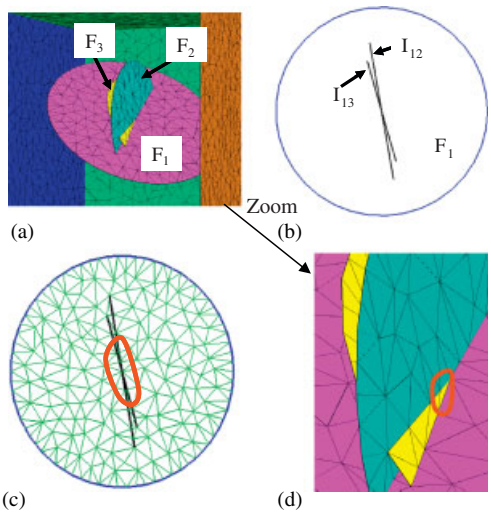

Figure 13. (a) Presents a three-fracture configuration. F_1 intersects F_2 and F_3 along a small angle (b); degenerate triangles are generated in (c) between the intersections and in a zoom of (a) as shown in (d).

second case) and Figures 13(c) and (d). In this case, a mesh refinement technique can be used for representing 3D objects with critical and complex configurations. However, mesh refinement may not be practical especially for highly complex fractured media. Thus, Step 3 in the developed method is essential for analyzing complex and critical configurations.

3. NUMERICAL EXAMPLES

This section presents examples of fracture networks. First, single-fracture configurations (Figures 14(a) and (b)) are used to validate the approach using a finite-volume method for simulating a solute transport problem. Then, solute transport simulations with a more complex configuration (Figure 14(c)) are presented. All numerical simulations presented here are completed with the HydroGeoSphere model [36, 37]. The governing equations can be found in [38] and are not repeated here. The method of solution for both flow and transport problems is based on the control volume finite element approach [36, 37, 39, 40]. The basic idea of the control volume finite element approach is to obtain a discretized equation that mimics the governing mass conservation equation locally. A volume of influence, referred to as a control volume, is assigned to each node. The discretized equation for a given node then consists of a term describing the change in fluid mass storage for that volume that is balanced by the term representing the divergence of the fluid

DOI: 10.1002/fld

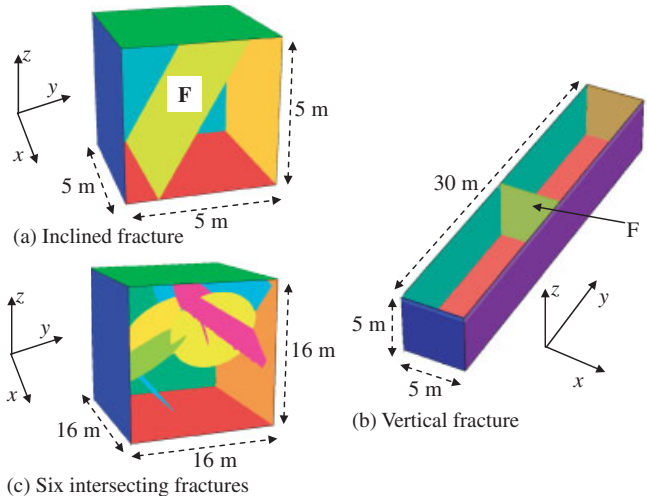

Figure 14. Fractured media used in the numerical examples. (a) Example 1: inclined fracture embedded in an impermeable matrix to compare flow results with the analytical solution by Otaga and Banks [34]; (b) Example 2: vertical fracture embedded in a porous matrix to compare flow results with the analytical solution by Tang *et al.* [35]; (c) Example 3: fracture network stochastically generated and embedded in a porous matrix for testing in complex and intersecting fractures.

mass flux in the volume. The fluid mass flux will depend on the physical properties associated with the volume and the difference in the value of the primary variable between the node in question and its neighbors. The governing equations for solute transport are identical to those used by Graf and Therrien [27]. A detailed description of the model can be found elsewhere [36].

3.1. Example 1. Solute transport in an inclined fracture embedded in an impermeable matrix

In this example, the model domain is a cube with a side length of 5 m. The cubic domain is considered to be impermeable, except for a single fracture F shown in Figure 14(a). The lateral boundaries of the fracture are impermeable and the top and bottom boundaries of the fracture are assigned constant hydraulic heads to create a uniform flow field. The top boundary of the fracture is assigned a constant solute source of relative concentration $c=1$. The prescribed boundary conditions are chosen to force 1D advective–dispersive–diffusive solute transport along the fracture, allowing comparison with the Ogata–Banks [34] analytical solution. Fluid flow and solute transport parameters are identical to those used by Shikaze *et al.* [24] and are listed in Table I.

Different gridding levels (fine: level 1; coarse: level 2) are generated using the SP method. The single-fracture configuration is a simple fractured medium that does not contain critical configurations. Consequently, the method will generate a mesh of adequate quality if the simplification procedure is utilized or not. However, SP method is used in this example to show that the adjustments made will (1) better control the mesh, and (2) not affect the solute transport results.

Simplifications using the SP method with three different elementary cubes (Table II) are applied. Table II shows different side lengths (h') of the small cube shown in Figure 11 that is used to analyze the critical configurations in the mesh of the fracture. Note that, a critical configuration is encountered in case 3 in Figure 13. This is because there are no constraints on the geometry of fracture F and, therefore, no inadequate triangles will be generated in Steps 1 and 2. For cases 1, 2 and 3 (Table II), Table III summarizes the number of tetrahedrons (# tetra), triangles (# trian), nodes (# node), the smallest edge and face's angle, the longest edge and largest face's angle for both grid levels. Table III shows that using the SP method and increasing h', the number of tetrahedrons decreases, the smallest edge side increases, and the smallest and largest face angles are closer to 60°. In addition, the longest edge is not changed because the SP method only analyzes small element sizes. The concentration profiles are shown in Figures 15 and 16. These figures with Figure 17 demonstrate good agreement between the analytical [38] and numerical solutions

DOI: 10.1002/fld

Table I. Model parameters used for the analysis of flow and solute transport in 3D (Example 3). All parameter values are identical to those used by Shikaze *et al*. [24]. Example 1.

Parameter	Value
Free-solution diffusion coefficient	$5\times10^{-9}\,\mathrm{m^2\,s^{-1}}$
Water density	$1000\,\mathrm{kg\,m^{-3}}$
Water viscosity	$1.1\times10^{-3}\,\mathrm{kg\,m^{-1}\,s^{-1}}$
Specific storage of matrix	$9.96\times10^{-5}\,\mathrm{m^{-1}}$
Matrix permeability	$10^{-15}\,\mathrm{m^2}$
Matrix longitudinal dispersivity	0.1 m
Matrix transverse dispersivity	0.005 m
Matrix porosity	0.35
Tortuosity	0.1
Specific storage of fracture	$4.32\times10^{-6}\,\mathrm{m^{-1}}$
Fracture dispersivity	0.1 m
Fracture aperture	50 μm

Table II. Simplifications using the SP method for two different grid levels; h' is the side length of the small cube shown in Figure 11. Example 1.

	Case 1	Case 2	Case 3
Grid level 1			
h' (m)	0.10	0.15	0.25
Grid level 2			
h' (m)	0.20	0.30	0.50

Table III. Number of tetrahedrons, triangles, nodes, smallest edge and face's angle, the longest edge and largest face's angle for both fine (grid level 1) and coarse (grid level 2) mesh of the inclined fracture. Example 1.

	# tetra	# trian	# node	Smallest edge (m)	Longest edge (m)	Smallest face angle (degree)	Largest face angle (degree)
Grid level 1							
SP method—Case 1	13 384	4318	2762	0.11	1.45	49.2	87.2
SP method–Case 2	12 987	4192	2670	0.19	1.45	54.3	77.3
SP method—Case 3	10 987	3832	1875	0.23	1.45	58.3	72.3
Grid level 2							
SP method—Case 1	6851	2724	1597	0.21	1.75	45.2	93.8
SP method—Case 2	5363	2304	1106	0.32	1.75	49.8	81.5
SP method—Case 3	3863	1704	701	0.43	1.75	53.7	75.1

proving that the numerical model correctly simulates flow and transport in fractured porous media. The results are accompanied with about 75% gain in memory capacity and CPU time; this can be seen by comparing the SP method in Case 1 (grid level 1) and Case 3 (grid level 2). Then, the SP method improves the mesh quality and reduces the CPU time while providing sufficiently precise numerical solutions.

3.2. Example 2. Solute transport in a fracture embedded in a porous matrix

In this example, we compare SP method and the analytical solution of solute transport for a single fracture in a porous matrix presented by Tang *et al.* [35]. This example simulates advection in the fracture, molecular diffusion in both fracture and matrix and fracture–matrix diffusion in a

DOI: 10.1002/fld

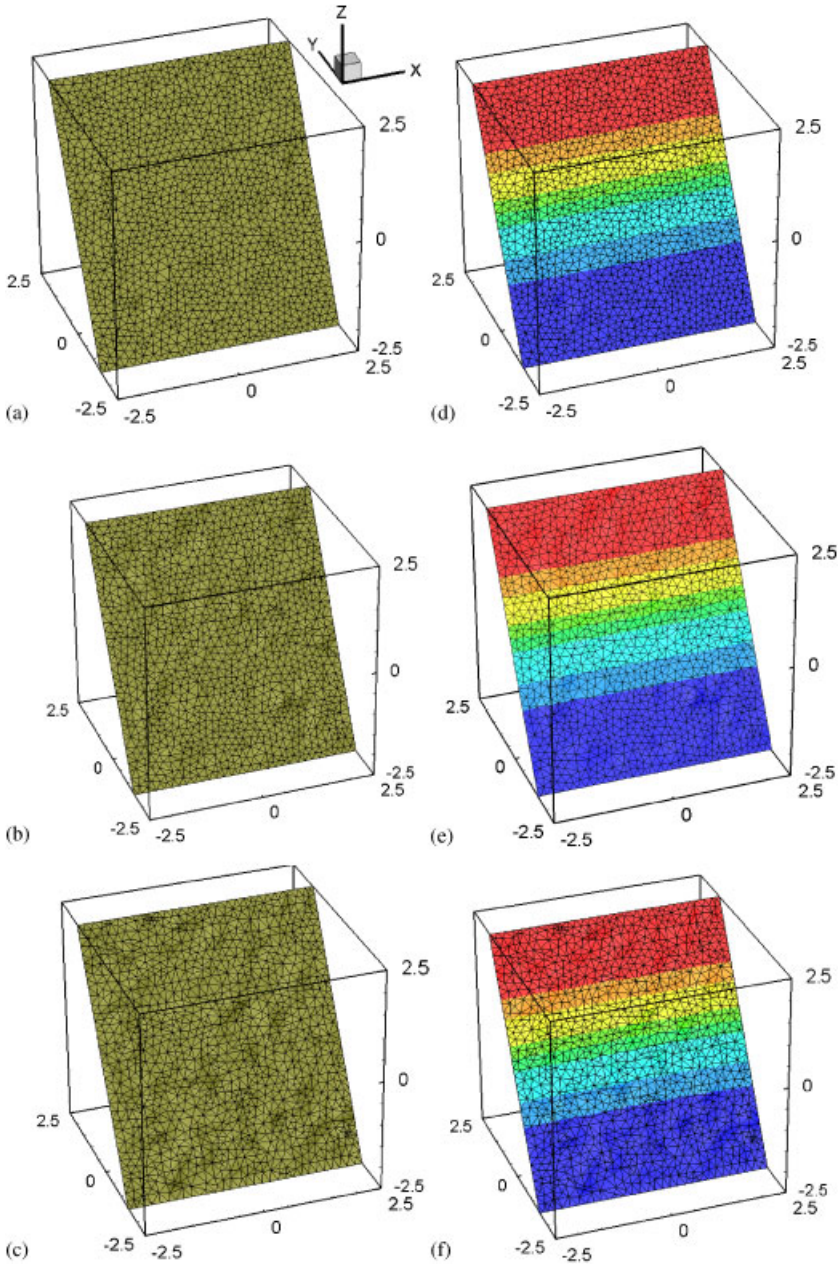

Figure 15. Solute transport simulation in a single inclined fracture. (a), (b) and (c) three levels of simplification using the SP method. (d), (e) and (f) solute transport using the mesh in (a), (b) and (c), respectively. Cube with 5 m length side. Grid level 1 (fine mesh), Example 1.

transient regime. The model domain is a parallelepiped ($5\,\mathrm{m} \times 30\,\mathrm{m} \times 5\,\mathrm{m}$) as shown in Figure 14(b). One fracture is located at $y = 0$. No flow (or solute flux) boundary conditions are imposed on all boundaries except the top and bottom boundaries where specified heads are applied such that the downward groundwater flow velocity in the fracture is constant ($0.01\,\mathrm{m\,day^{-1}}$). A specified concentration of 1 is imposed at the fracture top. Flow and transport parameters are summarized in Table IV.

SP method is used to generate two grid levels. For each grid level, a side length (h') of the small cube (Figure 11) is used to analyze the critical configurations (Table V). Table VI presents the information related to the grids used in this example. The system size (memory capacity and

DOI: 10.1002/fld

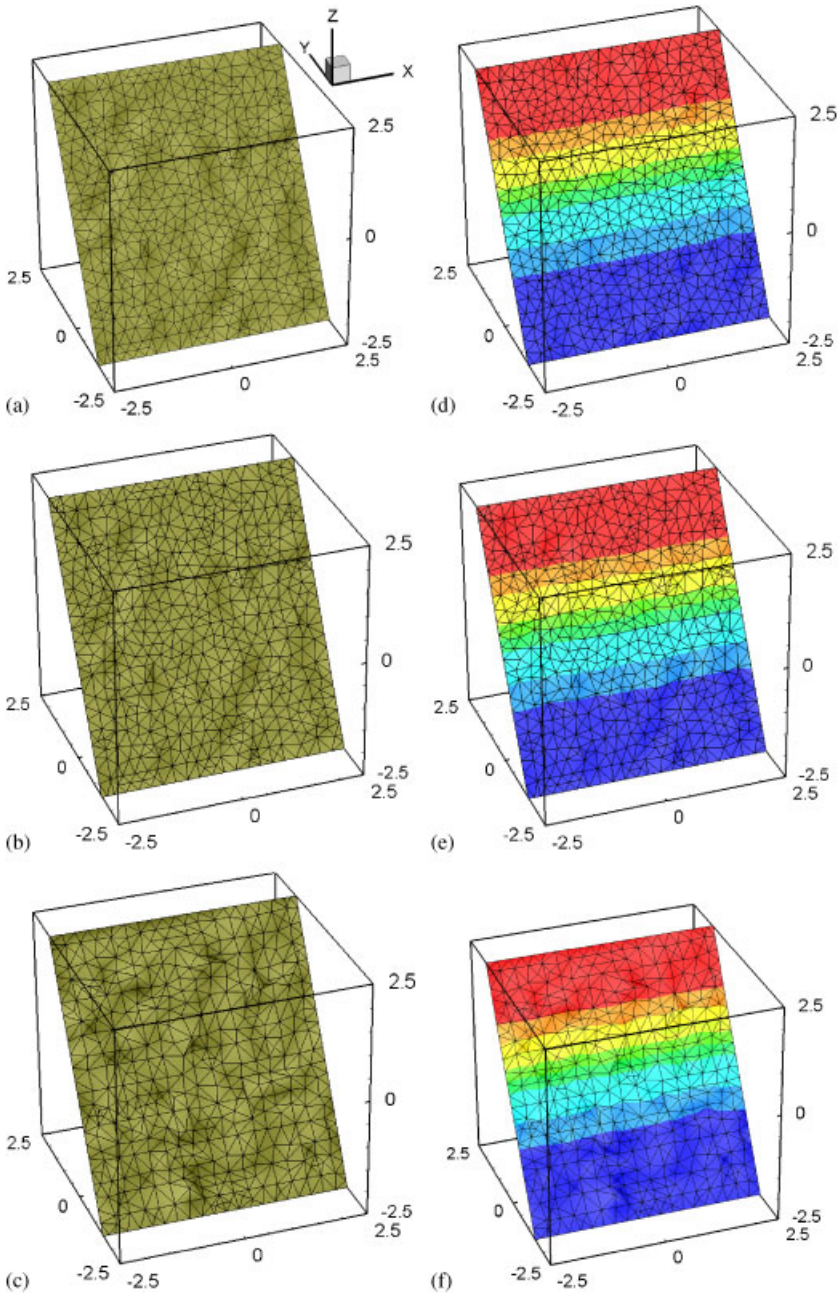

Figure 16. Solute transport simulation in a single inclined fracture. (a), (b) and (c) three levels of simplification using the SP method. (d), (e) and (f) solute transport using the mesh in (a), (b) and (c), respectively. Grid level 2 (coarse mesh), Example 1.

CPU time) is significantly reduced by using SP method. In addition, the mesh quality is shown in Table VI where all face angles are within the range $[50^\circ, 90^\circ]$ for both grid levels 1 and 2. The concentration profiles obtained using the finest mesh (Table VI) and grid level 2 with the SP method are very similar as shown in Figure 18. As in Example 1, the SP method produces similar results shown by the concentration profiles at the outlet for the solute transport in Figure 19. This figure also shows that the numerical solutions are in good agreement with the analytical solution by Tang *et al.* [35]. Note that, computational costs are about 60% less using the SP method for Grid level 2.

DOI: 10.1002/fld

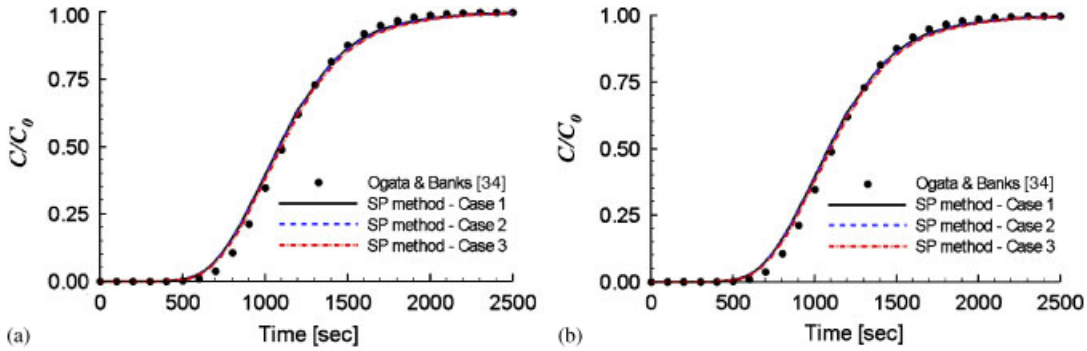

Figure 17. Concentration at the outlet for inclined fracture within an impermeable matrix. Analytical solution by Ogata and Banks [34] and numerical solutions using the SP method are shown for (a) grid level 1 and (b) grid level 2. Example 1.

Table IV. Model parameters used to verify solute transport in a fracture embedded in a porous low-permeability matrix. Example 2.

Parameter	Value
Matrix porosity	0.01
Matrix tortuosity	0.1
Free-solution diffusion coefficient	$1.6 \times 10^{-9}\,\mathrm{m^2\,s^{-1}}$
Half-life of solute (tritium)	0.0 year
Fracture dispersivity	0.0 m
Fracture groundwater velocity	$0.01\,\mathrm{m\,day^{-1}}$
Fracture aperture	100 μm

Table V. Simplifications using the SP method for two different grid levels; h' is the side length of the small cube shown in Figure 11. Example 2.

Grid level 1	
h' (m)	0.4
Grid level 2	
h' (m)	0.6

Table VI. Number of tetrahedrons, triangles, nodes, smallest edge and angle, longest edge and largest angle for a reference mesh (finest mesh), grid level 1 and grid level 2 of a fracture embedded in a porous low-permeability matrix. Example 2.

	# tetra	# trian	# node	Smallest edge (m)	Longest edge (m)	Smallest face angle (degree)	Largest face angle (degree)
Reference mesh							
SP method—without Step 3	9502	4457	2522	0.11	2.81	45.6	75.1
Grid level 1							
SP method	7166	3656	2027	0.41	3.02	55.3	81.5
Grid level 2							
SP method	4051	2560	1383	0.62	3.98	53.2	89.2

3.3. Example 3. Solute transport in a fracture network embedded in a porous matrix

In this example, a stochastically generated network of connected fractures (Figure 14(c)) embedded in a low-permeability porous matrix is considered. The domain is a cube with a side length of 16 m. Fluid flow and solute transport parameters are identical to those used by Shikaze *et al*. [24]

DOI: 10.1002/fld

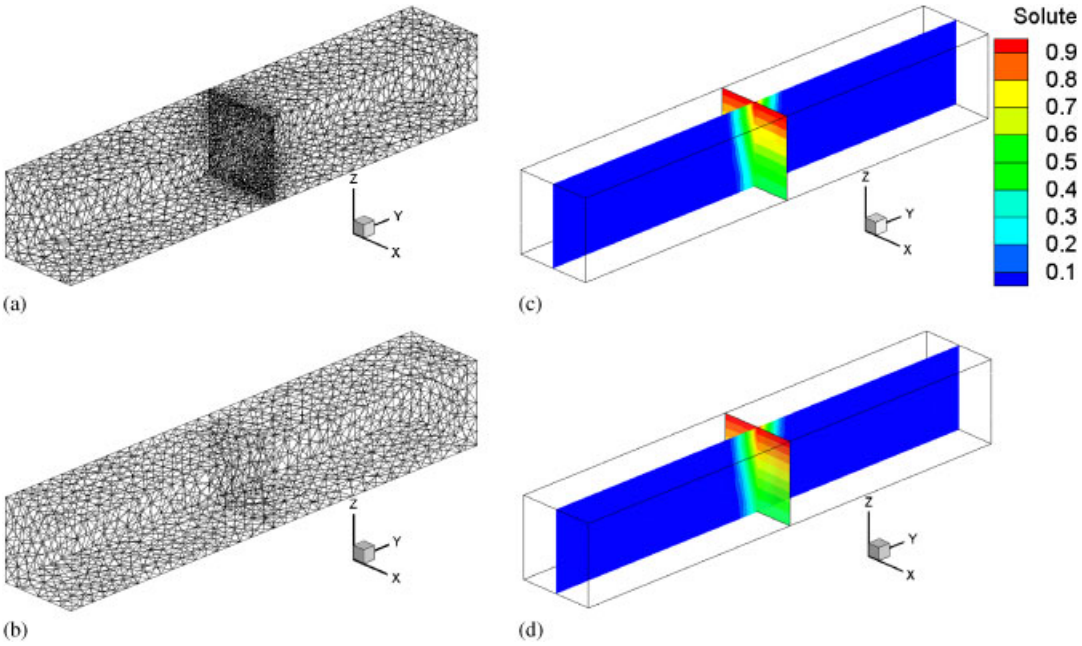

Figure 18. Solute transport simulation in a fracture embedded in a porous low-permeability matrix. (a) is a reference mesh (finest mesh in Table VI) using the SP method without including Step 3; (b) is a simplification of grid level 2 (Table VI) using the SP method. (c) and (d) are the solute transport using the mesh in (a) and (b), respectively. Example 2.

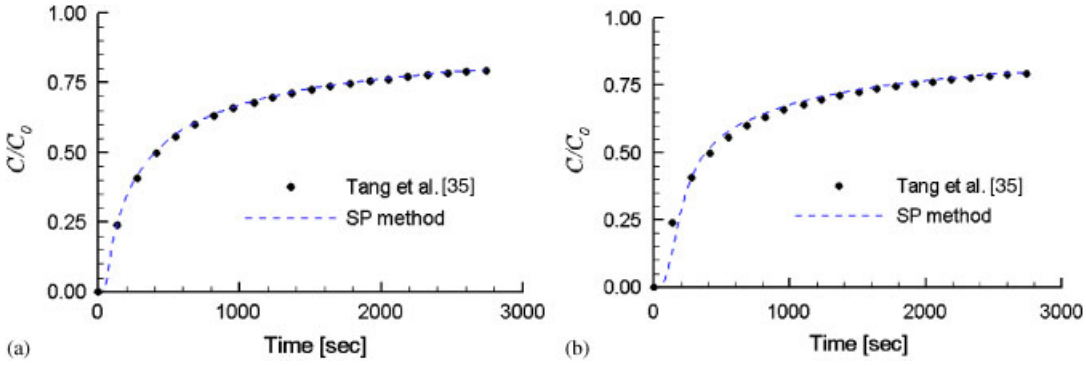

Figure 19. Concentration at the outlet in a vertical fracture embedded in a porous low-permeability matrix. Analytical solution by Tang *et al*. [35] and numerical solutions using SP method are shown for (a) grid level 1 and (b) grid level 2. Example 2.

and are listed in Table I. Parameters for the SP method are summarized in Table VII for two grid levels. These grids are listed in Table VIII.

A reference mesh with 98 047 tetrahedrons is generated without using the SP method to produce a numerical reference solution. With the grid level 2 (Table VIII), SP method generates 18 597 tetrahedrons and a mesh quality that can be read from the range of face angles. The concentration profiles calculated using this grid level are very close to the reference solution calculated from the finest mesh as shown in Figure 20. Moreover, the mesh obtained by the SP method (Grid level 2) is about 80% smaller than the reference mesh. Consequently, computational costs are reduced with about 80%.

For grid level 1, the concentration profiles at the outlet are similar and in agreement with the reference solution as shown in Figure 21(a). This figure shows that the SP method is an appropriate

DOI: 10.1002/fld

Table VII. Simplifications using the SP method for two different grid levels; h' is the side length of the small cube shown in Figure 11. Example 3.

Grid level 1	
h' (m)	0.3
Grid level 2	
h' (m)	0.5

Table VIII. Number of tetrahedrons, triangles, nodes, smallest edge and angle, longest edge and largest angle for a reference mesh (finest mesh), grid level 1 and grid level 2 of a fracture embedded in a porous low-permeability matrix. Example 3.

	# tetra	# trian	# node	Smallest edge (m)	Longest edge (m)	Smallest face angle (degree)	Largest face angle (degree)
Reference mesh							
SP method—without Step 3	98 047	32 985	21 153	0.11	2.1	58.6	76.5
Grid level 1							
SP method	51 203	20 124	11 930	0.32	3.02	52.2	82.2
Grid level 2							
SP method	18 597	7909	4580	0.53	3.99	49.2	86.2

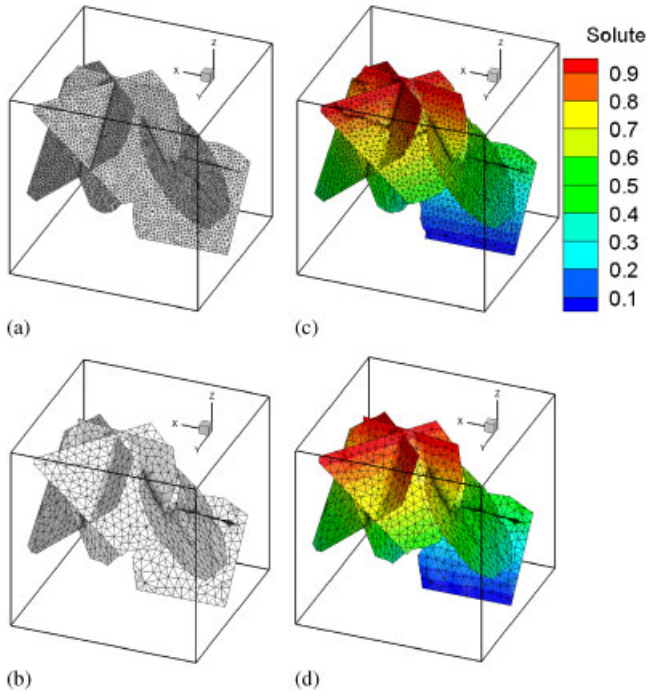

Figure 20. Simulation of solute transport in a fracture network embedded in a low-permeability porous matrix. (a) reference mesh (fine mesh) without using Step 3; (b) one-level simplification of grid level 2 (Table VIII) using the SP method. (c) and (d) solute transport using the mesh in (a) and (b), respectively. Example 3.

method when working with coarse grids; this is mainly because of the ability of the method developed to control the mesh to generate optimal elements. Here, the method adjusts the grids to converge towards the reference solution.

DOI: 10.1002/fld

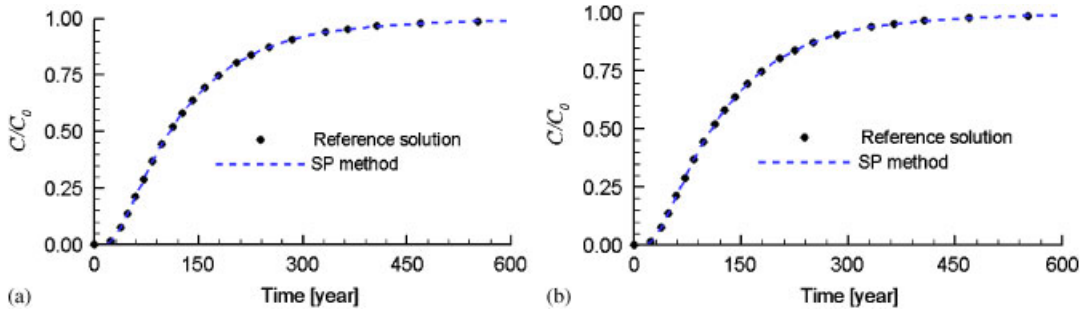

Figure 21. Concentration at the outlet for the intersecting fractures within an impermeable matrix. The reference solution and numerical solutions using the SP method are shown for (a) grid level 1 and (b) grid level 2. Example 3.

4. CONCLUSIONS AND DISCUSSION

This paper presents a method designed to discretize 3D complex fractured media for subsurface flow and solute transport simulations. The key idea of the approach is to transform locally critical geometric configurations in fractured media. The method: (1) removes some of the tetrahedrons by analyzing the triangulations of the fractures, and provides a mesh quality; (2) approximately maintains the geometric integrity of the input surfaces and geological data. Intersections between fractures may only generate critical configurations. In that case, areas of fractures will marginally change after applying the method and very close configurations are obtained after removing the critical complexities; (3) allows the inclusion of a refinement procedure, for example, to locally adapt the mesh of complex configurations of fractured clusters; this is shown by generating fine triangulation in the fractures and coarse for the domain's borders. Consequently, different gridding densities (close to fractures and far from fractures) will be generated; (4) provides precise numerical solutions. Using simple configurations of single inclined and regular fracture, the method is shown to give results in agreement with analytical solutions by Ogata and Banks [34], and Tang *et al*. [35]. Comparing to a reference solution obtained on finer grids of a complex fractured domain, the method improves the numerical results and fits for coarse grids; (5) analyzes the complexities extremely well, while slightly modifying the initial configurations to provide an optimal mesh; (6) is numerically stable in the sense that the solution obtained is exactly the reference solution, when no critical configurations are in the fractured media geometry and (7) is computationally efficient because it reduces computational costs by about 80% for the examples presented.

The method presented in this work is tested on synthetically generated examples. More realistic fractured media including fractured reservoirs and aquifers will be discretized in a future work for enhancing oil/gas recovery and understanding fundamental mechanisms for CO_2 sequestration.

REFERENCES

1. Bonnet E, Bour O, Odling NE, Davy P, Main I, Cowie P *et al*. Scaling of fracture systems in geological media. *Reviews of Geophysics* 2001; **39**:347–383.
2. Berkowitz B. Characterizing flow and transport in fractured geological media: a review. *Advances in Water Resources* 2002; **25**:861–884.
3. Desbarats AJ, Dimitrakopoulos R. Geostatistical modeling of transmissibility for two-dimensional reservoir studies. *SPE Formation Evaluation* 1990; **5**:437–443.
4. Dimitrakopoulos R. Stochastic modeling of space dependant reservoir-rock properties. *The Journal of Canadian Petroleum Technology* 1991; **30**:43–51.
5. Dimitrakopoulos R, Desbarats AJ. Geostatistical modeling of grid block permeabilities for three-dimensional reservoir simulators. *SPE Reservoir Engineering* 1993; **8**:13–18.

DOI: 10.1002/fld

6. Dimitrakopoulos R. Stochastic methods for petroleum reservoir characterization and production forecasting. *Journal of the Japanese Association for Petroleum Technology* 1996; **61**:538–548.
7. Dowd PA, Xu C, Mardia K, Fowell RJ. A comparison of methods for the stochastic simulation of rock fractures. *Mathematical Geology* 2007; **39**:697–714.
8. Silliman SE, Berkowitz B. The impact of biased sampling on the estimation of the semivariogram within fractured media containing multiple fracture sets 1. *Mathematical Geology* 2000; **32**:543–560.
9. Michael S, Riley M. An algorithm for generating rock fracture patterns: mathematical analysis. *Mathematical Geology* 2004; **36**:683–702.
10. Frey PJ, George PL. *Mesh Generation*: *Application to Finite Elements*. Hermes Science Publishing: Oxford, Paris, 2000; 816.
11. Reichenberger V, Jakobs H, Bastian P, Helmig R. A mixed-dimensional finite volume method for two-phase flow in fractured porous media. *Advances in Water Resources* 2006; **29**:1020–1036.
12. Hoteit H, Firoozabadi A. Numerical modeling of diffusion in fractured media for gas injection and recycling schemes. *SPE Journal* 2009; 323–337.
13. Karimi-Fard M, Firoozabadi A. Numerical simulation of water injection in fractured media using the discretefracture model and the Galerkin method. *SPE Reservoir Evaluation and Engineering* 2003; **6**:117–126.
14. Karimi-Fard M, Durlofsky LJ, Aziz K. An efficient discrete fracture model applicable for general purpose reservoir simulators. *SPE Journal* 2004; **9**:227–236.
15. Hoteit H, Firoozabadi A. Compositional modeling by the combined discontinuous Galerkin and mixed methods. *SPE Journal* 2006; **11**:19–34.
16. Monteagudo J, Firoozabadi A. Control-volume model for simulation of water injection in fractured media: incorporating matrix heterogeneity and reservoir wettability effects. *SPE Journal* 2007; **12**:355–366.
17. Graf T, Therrien R. A method to discretize non-planar fractures for 3D subsurface flow and transport simulations. *International Journal for Numerical Methods in Fluids* 2008; **56**:2069–2090.
18. Andersson J, Dverstorp B. Conditional simulations of fluid flow in three-dimensional networks of discrete fractures. *Water Resources Research* 1987; **23**:1876–1886.
19. Cacas MC, Ledoux E, de Marsily G, Tillie B, Barbreau A, Durand E, Fuega B, Peaudecerf P. Modeling fracture flow with a stochastic discrete fracture network: 1. The flow model. *Water Resources Research* 1990; **26**:479–489.
20. Cacas MC, Ledoux E, De Marsily G, Barbreau A, Calmels P, Gaillard B, Margritta R. Modeling fracture flow with a stochastic discrete fracture network: 2. The transport model. *Water Resources Research* 1990; **26**:491–500.
21. Mustapha H, Mustapha K. A new approach to simulating flow in discrete fracture networks with an optimized mesh. *SIAM Journal on Scientific Computing* 2007; **29**:1439–1459.
22. Moenickes S, Taniguchi T, Kaiser R, Zielke W. A 2.75D finite element model of 3D fracture network systems. *Proceedings of the 11th International Meshing Roundtable*, Sandia National Laboratories, Ithaca, NY, U.S.A., September 2002; 161–168.
23. Therrien R, Sudicky EA. Three-dimensional analysis of variably saturated flow and solute transport in discretely-fractured porous media. *Journal of Contaminant Hydrology* 1996; **23**:1–44.
24. Shikaze SG, Sudicky EA, Schwartz FW. Density-dependent solute transport in discretely-fractured geologic media: is prediction possible? *Journal of Contaminant Hydrology* 1998; **34**:273–291.
25. Krasovec ML, Burns DR, Willis ME, Chi S, Toksoz MN. 3-D finite difference modeling for borehole and reservoir applications. Earth Resources Laboratory, Department of Earth, Atmospheric, and Planetary Sciences, Massachusetts Institute of Technology, Cambridge, MA, U.S.A., 2004; 15.
26. Watanabe K, Takahashi H. Fractal geometry characterization of geothermal reservoir fracture networks. *Journal of Geophysical Research* 1995; **100**(B1):521–528.
27. Graf T, Therrien R. Variable-density groundwater flow and solute transport in porous media containing nonuniform discrete fractures. *Advances in Water Resources* 2005; **28**:1351–1367.
28. Normani SD, Sykes JF, Sudicky EA, Park Y-J. Palaeo-evolution and uncertainty analysis of regional groundwater flow in discretely fractured crystalline rock. In *Calibration and Reliability in Groundwater Modelling*: *From Uncertainty to Decision Making*, *Proceedings of Model CARE'2005*, Bierkens MFP, Gehrels JC, Kovar K (eds). The Hague, Netherlands, 2005; IAHS Publication No. 304, ISBN 1-901502-58-9, 2006; 180–186.
29. Blessent D, Therrien R, Macquarrie K. Coupling geological and numerical models to simulate groundwater flow and contaminant transport in fractured media. *Computers and Geosciences* 2009; **35**:1897–1906.
30. Mustapha H, Dimitrakopoulos R. Discretizing two-dimensional complex fractured fields for incompressible two-phase flow. *International Journal for Numerical Methods in Fluids* 2009; DOI: 10.1002/fld.2197.
31. Delaunay Boris N. 'Sur la Sphere' vide. Izvestia akademia nauk SSSR, VII seria. *Otdelenie Matematicheskii i Estestvennyka Nauk* 1934; **7**:793–800.
32. George PL, Borouchaki H. *Delaunay Triangulation and Meshing*: *Applications to Finite Element*. Hermes: Paris, 1998; 413.
33. Chrisochoides N, Nave D. Parallel Delaunay mesh generation kernel. *International Journal for Numerical Methods in Engineering* 2003; **58**:161–176.
34. Ogata A, Banks RB. A solution of the differential equation of longitudinal dispersion in porous media. U.S. Geological Survey. *Technical Report 411-A*, Professional Paper, 1961.
35. Tang DH, Frind EO, Sudicky EA. Contaminant transport in fractured porous media: analytical solution for a single fracture. *Water Resources Research* 1981; **17**:555–564.

36. Therrien R, McLaren RG, Sudicky EA. HydroGeoSphere—a three-dimensional numerical model describing fully-integrated subsurface and surface flow and solute transport (Draft edn). Groundwater Simulations Group, University of Waterloo, 2009. Available from: http://www.science.uwaterloo.ca/∼mclaren/public/hydrosphere.pdf.
37. Therrien R, Sudicky EA. Three-dimensional analysis of variably saturated flow and solute transport in discretely fractured porous media. *Journal of Contaminant Hydrology* 1996; **23**:1–44.
38. Bear J. *Dynamics of Fluids in Porous Media*. Elsevier: New York, 1972, 784.
39. Forsyth PA. A control volume finite element approach to NAPL groundwater contamination. *SIAM Journal on Scientific and Statistical Computing* 1991; **12**:1029–1057.
40. Forsyth PA, Simpson RB. A two phase, two component model for natural convection in a porous medium. *International Journal for Numerical Methods in Fluids* 1991; **12**:655–682.

DOI: 10.1002/fld